PROCEEDINGS OF SCIENCE

Thermal and Non-thermal emission study in GRB160709

Donggeun Tak*
University of Maryland
NASA Goddard Space Flight Center
E-mail: takdg123@umd.edu

Sylvain Guiriec
The George Washington University
NASA Goddard Space Flight Center
E-mail: sylvain.guiriec@gmail.com

Z. Lucas Uhm
NASA Goddard Space Flight Center
E-mail: z.lucas.uhm@gmail.com

Nicola Omodei
Stanford University
E-mail: nicola.omodei@stanford.edu

Julie McEnery
NASA Goddard Space Flight Center
University of Maryland
The George Washington University
E-mail: julie.mcenery@nasa.gov

GRB160709A is one of the small sample of short Gamma-ray Bursts detected by both the Gamma-ray Burst Monitor and the Large Area Telescope on-board the *Fermi* Gamma-ray Space Telescope. We performed a detailed spectral analysis of the Fermi gamma-ray data for this GRB. The spectrum is well described by a combination of thermal and non-thermal spectral components. The lightcurve of this GRB can be described by several phases: a weak precursor, an intense main peak and a weak tail. In a time-resolved analysis of the main peak, we found evidence of a period dominated by thermal emission with a temperature of $\sim$340 keV. In addition to the spectral components dominating the low energy gamma-ray range, a hard power-law component with constant photon index is required to adequately describe the data at high energies. This extra component is present from the main peak through the weak tail. The flux of this component decreases with time, similar to the behavior seen in the bright short GRB090510 [1].

35th International Cosmic Ray Conference
10-20 July, 2017
Bexco, Busan, Korea

*Speaker.

PoS(ICRC2017)643

1. Introduction

Gamma-ray Bursts (GRBs) are among the most energetic emission events in the universe. They release huge amounts of energy, corresponding to the mass of sun, within milliseconds to hours. These explosive events have been studied since the late 1960s. GRBs are classified into two categories, long duration GRB (T_{90}[1]>2s) and short duration GRB (T_{90}<2s). They are believed to be powered by different progenitors. Generally short GRBs is modeled with a merger of two compact objects [2], whereas long GRBs come from collapse of a massive star [3]. The temporal and spectral features of long and short GRBs show differences as well as commonalities (see Zhang et al.(2016)[4] for a recent observational review).

GRBs have two phases, prompt emission and afterglow. The prompt emission is a short but intense emission phase lasting few seconds and the afterglow is a long-lived time-decaying emission phase with broad energy range from X-ray to radio. In most cases, prompt emission of GRB is dominant in gamma-ray energy band (kev-MeV). In this energy band, prompt emission spectra of GRBs have been well described by a representative empirical model, Band function [5]; a smoothly broken power law with low (α) and high (β) energy spectral indices. Generally Band function describes non-thermal emission spectra. The energy spectra of synchrotron radiation, commonly used to model prompt gamma-ray emission, has an limit on its spectral index. A low energy spectral index α from any population of electrons has to be equal or softer than -2/3 corresponding to the spectral index of a single electron radiation [7]. The observed spectral index values of α spread over the wide range and many cases having a low spectral index harder than -2/3 are observed. This challenges synchrotron emission alone model. Also along with the non-thermal component (Band), an additional power-law component, or a sub-dominant thermal component is reported in several GRBs (e.g. GRB090510 [1]; GRB100724B [8]). To describe these spectra, other emission models are proposed, but the fundamental emission mechanism of GRBs is still in debate (see Kumar & Zhang(2015)[9] for a recent GRB physics review)

Fermi Gamma-ray Space Telescope launched in June 2008 is an excellent tool for studying GRBs. *Fermi* has two instruments; the Gamma-ray Burst Monitor (GBM) and the Large Area Telescope (LAT). GBM consists of 12 sodium iodide (NaI, 8 keV - 1 MeV) and 2 bismuth germanate (BGO, 200 keV - 40 MeV) detectors. GBM is capable of observing the unocculted full sky with broad energy coverage and it specializes in detecting transient gamma ray events such as GRBs. LAT is a pair-conversion telescope that observes high energy photons above 30 MeV with a 2.4 steradian field of view. The GBM and LAT combined make it possible to achieve a seamless study of the prompt emission of GRBs over seven decades in energy. LAT has detected more than 120 GRBs with only 10% of them being short GRBs. Due to the paucity of short bright GRB, the high energy features of short GRB is not fully studied. Studies of GRB160709A help broaden our understanding of emission mechanisms of short gamma-ray bursts.

2. Observation

At 19:49:03.50 UT on 09 July 2016 (hereafter T_0), *Fermi*-GBM triggered on and located

[1] T_{90} refers time duration containing 90% of accumulated counts between 50 and 300 keV, T_{90}=T_{95}-T_{05}

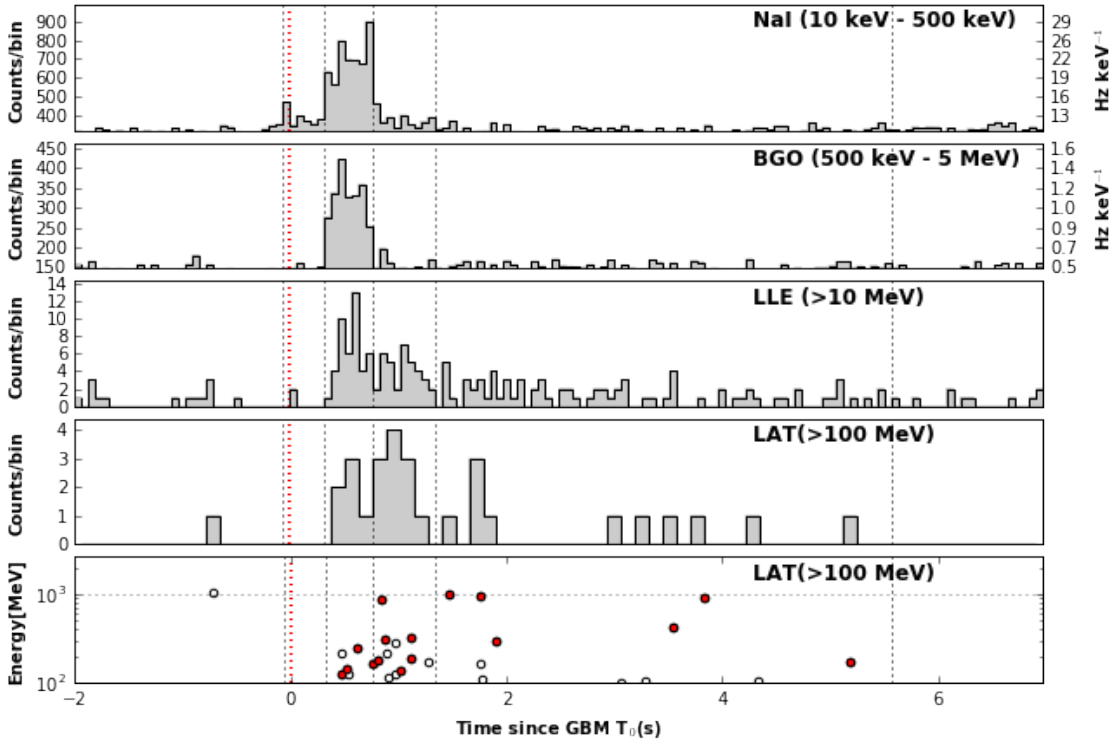

Figure 1: Composite light curve of GRB160709 in different energy ranges from lowest to highest with GBM and LAT. The bin size is 0.064 seconds for GBM and LLE, and 0.128 seconds for LAT. In the bottom, all LAT event energies are plotted as function of time. Red filled circles are the events highly regraded as coming from GRB160709A (>90%). The red vertical line represents GBM trigger time (T_0). They are separated by black dotted lines at T0 + (-0.064, 0.320, 0.768, 5.568)s. The first and the last vertical lines mean T_{05} and T_{95} respectively.

GRB160709A. Even though *Swift*-BAT was not triggered due to its sub-threshold detection, the ground analysis found a 8.8 sigma detection and localized GRB160709A with high precision (R.A., Dec.) = (235.996, -28.188) with 0.04 error radius. *Fermi*-LAT also found the significant signal from the ground analysis and LAT Low-energy event (hereafter LLE, >10MeV) selection showed its high significant detection about 10 sigma. The prompt emission of GRB160709A is also reported by Konus-Wind, CALET, and ASTROSAT.

Figure 1 shows a composite light curve of GBM and LAT with different energy selections. GBM is triggered by a weak precursor, followed by the bright prompt emission and a long-lived tail of the prompt emission. The GBM T_{90} of GRB160709 is 5.632 +/- 1.286 sec, which is longer than the usual T_{90} of short GRB. This is because of the soft tail in cumulative photon fluence. The T_{50} of GRB160709 is 0.576 +/- 0.202 sec, which belongs to the short GRB category [10]. The LAT detected more than 20 events above 100 MeV within 30 seconds. The highest energy photon is 0.991 GeV, detected 1.467 sec after T_0. Based on the features in the light curve, we divided the time interval of T_{90} into four episodes. The first episode is the time interval from -0.064s (T_{05}) to 0.320s where the emission is noticeable only in the lower energy region. The second time interval, or the main episode from 0.320s to 0.768s, contains the bulk of the prompt emission in both GBM

and LLE energy ranges. The third episode from 0.768s to 1.344s is characterized by significance of high energy emission above 100 MeV, and the final episode from 1.344s to 5.536s (T_{95}) is the tail end of the prompt emission.

3. Spectral Analysis

3.1 Analysis method

We performed a time-resolved spectral analyses with GBM and LAT data. For the GBM, we used four NaI detectors (8 keV - 1 MeV) and two BGO detectors (200keV - 40 MeV). For the LAT, we used two selections, LLE (>10 MeV) and LAT (>100MeV). We use "*Transient100*" event class with applying a zenith angle cut of 100 degree. In GBM data, low and high channels are ignored due to instrumental non-linearities or overflow channels; for NaI 1-6 (low) and 126-128 (high) channels and for BGO 1-3 (low) and 125-128 (high) channels are ignored. In addition, there is a discontinuity in the response of the NaI detectors around 33.17 keV due to the Iodine K-edge, so the corresponding channels are ignored as well (22-28 channels). We used two spectral analysis tools *rmfit 4.3.2*[2] and *Xspec 12.9.1*[3]. We used *rmfit* for the initial analysis, and double-checked the results with *Xspec*. The background is fit by a polynomial with time intervals before and after the burst with *rmfit*. The time intervals used for the background estimation are [T_0-40, T_0-10]s and [T_0+20, T_0+60]s for NaI and BGO. For LLE, longer time intervals [T_0-250, T_0-50]s and [T_0+100, T_0+400]s are selected. The same background was also used in *Xspec* to maintain consistency. We fit various models; simple power law (PL), a power law with exponential cutoff (PL_{cutoff}), the Band function, a black body (BB) and combinations of these models. The best-fit model is determined by considering its test statistics and degrees of freedom compared to other models. We used a test statistics called PG-stats (Poisson data with a Gaussian background[4]) to fit the spectral data. In some cases, several models provided an equally good fit. We performed a simulation study with *Fakeit* to explore how these models might relate to one another. *Fakeit* is a tool for generating synthesized bursts based on a model with given parameters and adding Poisson fluctuations to the synthesized bursts. By using *Fakeit*, we generated synthetic spectra with the parameters given by one of model fits (the source model). We fit the synthetic spectra with each competing model including the source model. We repeated the procedure while changing the source model. From these simulation, We could get goodness of fit and trustworthiness of fit. Also we could test whether or not one model can reproduce parameters in other models. In this paper, we present *Xspec* results. The best-fit model for each time interval is the same for *rmfit* and *Xspec*, and the parameters agrees within 1 σ errors.

3.2 Time-integrated analysis for each episode

Figure 2 shows the best-fit models for each episode. The upper panel shows GBM light curve and LAT-detected event as function of energy and time. Each of the four episodes is depicted with

[2]rmfit, https://fermi.gsfc.nasa.gov/ssc/data/analysis/rmfit for detail

[3]Xspec, https://heasarc.gsfc.nasa.gov/xanadu/xspec for detail

[4]PG-stats, https://heasarc.gsfc.nasa.gov/xanadu/xspec/manual/XSappendixStatistics.html for detail

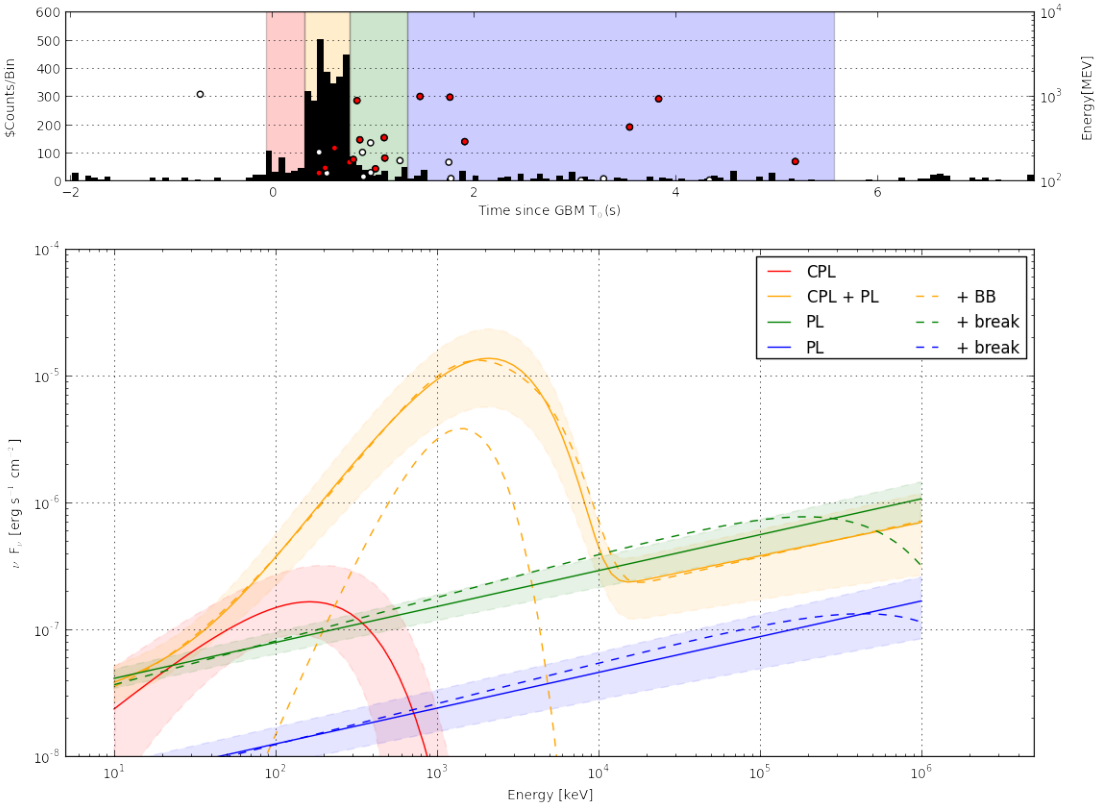

Figure 2: Spectral models of GRB160709 in different time intervals. In this figure, the best-fit models are plotted with 1σ error contours. The additional power law component starts to appear in the second main emission episode. Dashed models are alternative models for each region, which have almost the same PGstats but more degree of freedoms. Separated-yellow-dotted line represents probable blackbody component.

different colors for both light curve and spectra.

THE FIRST EPISODE (WEAK PRECURSOR): The best-fit model for the first episode is a power law with exponential cutoff. Compared to a simple power law, PG-stats difference is about 29 which corresponds 5.2 sigma. This is coherent with the light curve feature of the first episode that only low energy events are noticeable. Even though the best-fit model is $\mathrm{PL_{cutoff}}$, it is possible that we underestimated its complexity due to small number of events. The index of $\mathrm{PL_{cutoff}}$ is $-0.95^{+0.38}_{-0.31}$ with $\mathrm{E_{peak}}$ 163^{+82}_{-40}, which agrees with the typical low energy index of GRBs.

THE SECOND EPISODE (MAIN PEAK): We found some interesting features in this time interval. Unlike most GRBs, the Band function does not describe the prompt emission spectral shape of GRB160709A. A $\mathrm{PL_{cutoff}}$ with $\mathrm{PL_{extra}}$ ($\alpha = -0.19^{+0.08}_{-0.07}$; $E_{\mathrm{peak}} = 2092^{+117}_{-112}$; $\Gamma = -1.74^{+0.04}_{-0.04}$) is a better description of data than the Band function alone(ΔPG-stats $\sim$ 29, 5.4σ). We tried to add a $\mathrm{PL_{extra}}$ to the Band function, but β becomes very soft ($\leq$ -10) so that the Band function and $\mathrm{PL_{cutoff}}$ are indistinguishable. Adding a blackbody to a $\mathrm{PL_{cutoff}}$ improves PG-stats slightly $\sim$ 17 less preferred than $\mathrm{PL_{cutoff}}$ with $\mathrm{PL_{extra}}$. We also tested a model with three components; $\mathrm{PL_{cutoff}}$ with both $\mathrm{PL_{extra}}$ and blackbody. The lowest PG-stats is achieved with this three component model. However, ΔPGstat between the three component model and the two component model ($\mathrm{PL_{cutoff}}$ with $\mathrm{PL_{extra}}$)

is not enough to compensate for the increase of 2 degree of freedom (ΔPG-stats $\sim$ 2). We tried three components with fixing parameters as suggested by Guiriec et al.(2015)[11]; $\alpha = -0.7$ and $\Gamma = -1.5$. The PG-stats for this model is slightly higher than PL_{cutoff} with PL_{break} with the same degree of freedom. The three models, which are a two component model (PL_{cutoff} with PL_{extra}), a three component model (two component model with a blackbody) and a three component model with fixed parameters ($\alpha = -0.7$ and $\Gamma = -1.5$), are equally well-fit so we performed simulations to find a true model. We found that the three models resembles each other, and they can reproduce others results within 1 sigma. Even if the blackbody component exists, we cannot distinguish the component from other components. It is possible that a thermal component is dominant in a short amount of time so we searched for a blackbody emission in 64 ms binned time-resolved analysis of the main episode (Sec. 3.3).

THE THIRD AND FORTH EPISODES (WEAK TAIL OF PROMPT EMISSION): a weak tail of the prompt emission is shown in the light curve during the third and forth episodes. During these periods, the PL_{cutoff}, which was dominant in the previous episode, disappears and the indices of power law components remain almost constant ($\Gamma_{3rd} = -1.72^{+0.02}_{-0.02}$; $\Gamma_{4th} = -1.72^{+0.03}_{-0.03}$). Also the indices are similar to the index of PL_{extra} in the main episode. This suggests that the emission process producing the power law component is continuous during the prompt emission from the main episode to the tail end of the prompt emission. We tested for the existence of a break in the power law components by fitting a PL_{cutoff}. For the third time interval, adding the break improves PG-stats modestly (ΔPG-stats$\sim$ 8, 2.83σ). For the last time interval, the improvement of PG-stats is even smaller (ΔPG-stats$\sim$ 4, 2σ). These improvements are not sufficient to confirm the existence of the breaks so the breaks are less likely to exist in these time-intervals.

3.3 Time-resolved analysis for the main episode

We performed time-resolved analysis in the main episode with 64 ms time-binned intervals. We used PL_{cutoff} with PL_{extra}; when it is difficult to constrain PL_{extra} component due to low counts of events in high energy region, we used PL_{cutoff} without PL_{extra}. We selected this model because it was the best-fit model in both the time-integrated interval and in each time-resolved interval in most cases. Also it is easy to see the evolutions of each parameter.

Figure 3 shows the evolution of the indices of PL_{cutoff} and PL_{extra}, and E_{peak}. PL_{cutoff} index (α) changes significantly. At its maximum, the value of α is $\sim$ +0.8. This value is not well reproduced by synchrotron emission, because α produced by synchrotron mechanism has upper limit around -2/3[7]. However a blackboy, which is a thermal emission spectrum, show a harder spectral shape so we tested the blackbody to the two time-intervals when the indexes are $\sim$ +0.8. We could successfully fit them with the blackbody with PL_{extra} without significant changes in statistical goodness of fit. Statistically, the blackbody with PL_{extra} is the best fit because it has comparable PG-stats and fewer degree of freedom. This suggests that thermal emission dominates in these time-intervals with a temperature of about 340 keV. We tried to fit the three component model (PL_{cutoff}, BB and PL_{extra}) with α = -0.7 and Γ = 1.5 in these time intervals. However E_{peak} was not constrained because two components (PL_{cutoff} and BB) are overlapped. The simulation results of comparing the two component model and the fixed three component model were not conclusive as well. In other time intervals, the most of alpha index of PL_{cutoff} does not agree with both a synchrotron model ($\geq$ -2/3) and a blackbody ($\geq$ +1). One explanation is the consideration of the combination of thermal

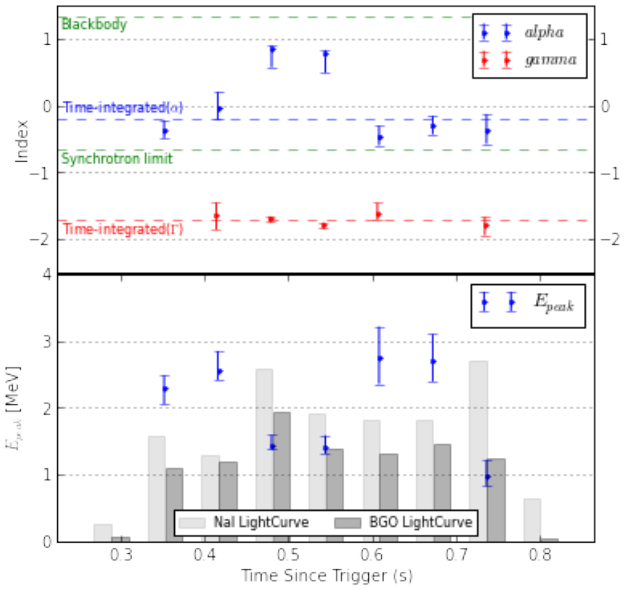

Figure 3: Evolution of indices and E_{peak} in the main emission interval. Top panel shows the evolutions of PL_{cutoff} index and PL_{extra} index, which are α and Γ respectively. The horizontal lines show the time-integrated best fit values (blue and red) and blackbody radiation and synchrotron radiation limit (green, 1.34 and -2/3 respectively). The bottom panel shows the evolution of E_{peak} and cumulative light curve of NaI (light gray) and BGO (dark gray).

and non-thermal emissions. Adding the blackbody to PL_{cutoff} tends to lower the index of PL_{cutoff}. For example, in 0.384-0.448s time-interval, adding a PL_{extra} to a PL_{cutoff} does not change the alpha index ($\Delta\alpha \sim$-0.05) significantly, but adding a blackbody component lowers the alpha index ($\Delta\alpha \sim$-0.43). In most cases, it is difficult to differentiate PL_{cutoff} and BB because one is laid on top of the other. Another possible explanation is to modify thermal or non-thermal spectrum by considering various effects such as temporal variability or multi-temperature blackbodies.

PL_{extra} index(Γ) is almost constant of $\sim$ -1.7. This value agrees with time-integrated result $-1.74^{+0.04}_{-0.04}$. This implies the emission process for PL_{extra} is independent of the emission process of PL_{cutoff}.

E_{peak} fluctuates significantly during the main episode. There are two drops; one is at about 0.45s and the other is at the end of the main peak emission. In the time interval right before the first drop occurs, the α index is in the middle of thermal and non-thermal expectation, $-0.03^{+0.25}_{-0.20}$. In this time interval, fixed 3 component model was well fitted without changing PG-stats. PL_{cutoff} is split into PL_{cutoff} with fixed α = -0.7 and BB. E_{peak} in PL_{cutoff} increases from 2500^{+106}_{-82} keV to 3265^{+1061}_{-1161} keV and the temperature in BB is about 530^{+106}_{-82} keV. The temperature of sub-dominant thermal component is consistent with that of dominant thermal component in following two time intervals. This continuity is more natural, and supports the idea that two components (thermal and non-thermal emissions) are overlapped in PL_{cutoff}. In addition to the first drop, there is another drop at the end. In contrast to the first drop, α index does not change. Also, high energy flux (BGO) rises in the first drop whereas low energy flux (NaI) rises in the second drop. These suggests that the origins of two phenomenons are distinct.

4. Summary

We have demonstrated the observational features of GRB160709A. GRB160709A is a unusual

short burst detected by both GBM and LAT, which allows us to analyze the burst in broad energy ranges. The spectra consists of several components including thermal components; PL_{cutoff}, PL_{extra} and Blackbody. This implies that GRB160709A is produced by not a single emission process but a multiple emission processes including both thermal and non-thermal emission processes. From this rare sample, we infer the complexity of Gamma-ray bursts. In summary, our observational analyses of the prompt emission of GRB160709A show following features:

1. GRB160709A triggered GBM with a weak soft precursor. This weak precursor is followed by the main peak emission, which lasts about 1 second. After the main peak emission, there was a weak tail of the prompt emission, which increases T_{90}.

2. We determined that unlike many bursts, a Band function is not the best description of the spectra of GRB160709A. The weak precursor is described by PL_{cutoff} with $\alpha \sim$ -1 and E_{peak} $\sim$ 163 keV. For the main peak emission, there are many well-fit models such as a model including a blackbody component for the spectral shape but the best-fit model is PL_{cutoff} with PL_{extra}. After the main emission, continous power law spectra are observed.

3. The observation of high energy events(LAT) are delayed compared to the lower energy events(GBM). This is likely to be related to the onset of extra power-law component, which starts to appear from the main peak emission and lasts until the end of the prompt emission without changing its spectral index.

4. In 64 ms time-binned analyses of the main peak, we found a evidence for the existence of thermal emission in GRB160709A. In several time intervals, the best-fit was BB with PL_{extra}, which is simultaneously well-fit by PL_{cutoff} with PL_{extra}. In these time-intervals, low spectral indices are ~ 0.8, which is more natural to be explained by a thermal emission. This suggests that a short thermal-dominated phase exists in the main peak emission.

5. We found that E_{peak} of PL_{cutoff} fluctuated significantly during the main peak emission. There are two significant drops in E_{peak}, and whenever the drop occurs, the flux rises noticeably. In the first drop, the spectral index of PL_{cutoff} increases abruptly. In the second drop, occurring at the end of the main peak emission, the spectral index remains unchanged but low energy flux rises. This implies that two events originated from different sources. The first drop might be related to the transition from sub-dominant to dominant thermal emission, but the latter might come from the release of the residual lower energy events produced by the emission process shaped PL_{cutoff}.

Acknowledgment The *Fermi*-LAT Collaboration acknowledges support for LAT development, operation and data analysis from NASA and DOE (United States), CEA/Irfu and IN2P3/CNRS (France), ASI and INFN (Italy), MEXT, KEK, and JAXA (Japan), and the K.A. Wallenberg Foundation, the Swedish Research Council and the National Space Board (Sweden). Science analysis support in the operations phase from INAF (Italy) and CNES (France) is also gratefully acknowledged. This work performed in part under DOE Contract DE-AC02-76SF00515.

References

[1] Ackermann, M., Asano, K., Atwood, W. B., et al. 2010, apj, 716, 1178

[2] Paczynski, B. 1986, apjl, 308, L43

[3] Woosley, S. E. 1993, apj, 405, 273

[4] Zhang, B., Lü, H.-J., & Liang, E.-W. 2016, ssr, 202, 3

[5] Band, D., Matteson, J., Ford, L., et al. 1993, apj, 413, 281

[6] Sari, R., Piran, T., & Narayan, R. 1998, apjl, 497, L17

[7] Preece, R. D., Briggs, M. S., Mallozzi, R. S., et al. 1998, apjl, 506, L23

[8] Guiriec, S., Connaughton, V., Briggs, M. S., et al. 2011, apjl, 727, L33

[9] Kumar, P., & Zhang, B. 2015, physrep, 561, 1

[10] Narayana Bhat, P., Meegan, C. A., von Kienlin, A., et al. 2016, apjs, 223, 28

[11] Guiriec, S., Kouveliotou, C., Daigne, F., et al. 2015, apj, 807, 148